ELSEVIER

International Journal of Solids and Structures 41 (2004) 3339–3352

INTERNATIONAL JOURNAL OF SOLIDS and STRUCTURES

www.elsevier.com/locate/ijsolstr

From constitutive modelling of a snow cover to the design of flexible protective structures Part II—Some numerical aspects

François Nicot *

Cemagref, Unité de Recherche Erosion Torrentielle Neige et Avalanches, Domaine Universitaire BP 76, 38402 Saint Martin d Heres, Grenoble, France

Received 5 February 2003; received in revised form 11 September 2003

Available online 27 February 2004

Abstract

The mechanical modelling proposed in Part I has led to the development of computational software allowing easy design of avalanche nets. This tool provides for the evolving forces acting on several parts of the net as a function of the snow situation. Some important numerical aspects are considered here, confirming the relevance of the proposed approach. To exemplify the capability of the software, a complete simulation is presented.

Keywords: Cable structures; Finite differences method; Snowpack

1. Introduction

The purpose of this second part is to establish that the Discrete–Lagrangian approach is particularly well adapted in the case of a snowpack in interaction with a flexible structure. The following results are inferred: first, it is shown that both the loading applied to the structure by the snowpack and its distribution between the poles and the anchors do not depend on the mechanical parameters (stiffness and viscosity) used in the constitutive model; second, the relevance of using large snow elements is properly established; and finally, a slight influence of the exponent α_{ice} is highlighted, justifying the adoption of linear constitutive modelling on the micro level between two grains in contact.

2. Influence of the mechanical parameters

Constitutive equations obtained in Part I (Eqs. (3), (43), (44) and (45)), in the general non-linear case, allow changes in the snowpack over time to be analysed. In order to exemplify the reasoning behind this

* Tel.: +33-4-76-76-27-70; fax: +33-4-76-51-38-03.
E-mail address: francois.nicot@grenoble.cemagref.fr (F. Nicot).

0020-7683/$ - see front matter © 2003 Elsevier Ltd. All rights reserved.
doi:10.1016/j.ijsolstr.2003.09.021

using only explicit analytical constitutive equations, the case of a local linear visco-elastic model (Maxwell fluid) is examined. In given meteorological conditions, the snowpack needs time to reach an equilibrium state. During this transient period, forces acting on the structure may change. It was assumed that the loading applied to the structure was maximal at the steady state. Once this state has been reached, the forces acting on the structure no longer change and are used to design the structure for this given snow situation. Hereafter, when a variable is considered at the steady state, the exponent (s) will be affixed.

At the steady state, Eq. (37) (Part I) can be rewritten as:

$$\bar{\sigma}_i^{(\mathrm{s})} = 2\eta_{\mathrm{ice}} C_{\mathrm{h}} \left(\overline{\overline{M^{(\mathrm{s})}}}_{i4} \overline{\overline{\dot{\varepsilon}^{(\mathrm{s})}}}_{12} + \overline{\overline{M^{(\mathrm{s})}}}_{i5} \overline{\overline{\dot{\varepsilon}^{(\mathrm{s})}}}_{13} \right) \quad (i = 1, \ldots, 6) \tag{1}$$

Components $\overline{\overline{M}}_{i4}$ and $\overline{\overline{M}}_{i5}$ only depend on function $\lambda(\theta, \varphi)$. From the definition of function $\lambda(\theta, \varphi)$, it appears that this function only depends on the maximum value of $\tilde{\sigma}(\theta, \varphi)$ which has never been reached: if this maximum value is equal to the limit stress $\tilde{\sigma}_l$, $\lambda(\theta, \varphi) = 1$, or $\lambda(\theta, \varphi) = 0$.

From the expression (Eq. (41), Part I) $\tilde{\sigma}(\theta, \varphi) = C_{12} \cos\theta \sin\theta \sin^2\varphi + C_{13} \cos\theta \cos\varphi \sin\varphi$, even though the two terms $\cos\theta \sin\theta \sin^2\varphi$ and $\cos\theta \cos\varphi \sin\varphi$ have the opposite sign when $\varphi \in [\frac{\pi}{2}; \pi]$, we admit that $\tilde{\sigma}(\theta, \varphi)$ is maximal when both C_{12} and C_{13} are also maximal. C_{12} and C_{13} are given by Eq. (42) (Part I), which can be rewritten as:

$$C_{1i} = 2\left(\frac{N_b^0}{N_g} \frac{\rho_s}{\rho_{\mathrm{ice}}} \right) \phi(\lambda) K_{\mathrm{ice}} \int_0^t \mathrm{e}^{\frac{K_{\mathrm{ice}}}{\eta_{\mathrm{ice}}}(\xi - t)} \overline{\overline{\dot{\varepsilon}}}_{1i} \, \mathrm{d}\xi \quad (i = 1, 2) \tag{2}$$

As $\overline{\overline{\dot{\varepsilon}}}_{1i}$ is a time-rising function, C_{1i} is also a time-rising function. Thus, C_{1i} is maximal at the steady state. Furthermore,

$$C_{1i}^{\max} = C_{1i}^{(\mathrm{s})} = 2\left(\frac{N_b^0}{N_g} \frac{\rho_s}{\rho_{\mathrm{ice}}} \right) \phi(\lambda) \eta_{\mathrm{ice}} \overline{\overline{\dot{\varepsilon}^{(\mathrm{s})}}}_{1i} \tag{3}$$

allowing the following expression of $\tilde{\sigma}^{\max}(\theta, \varphi)$ to be inferred:

$$\tilde{\sigma}^{\max}(\theta, \varphi) = 2\left(\frac{N_b^0}{N_g} \frac{\rho_s}{\rho_{\mathrm{ice}}} \right) \phi(\lambda) \cdot (\cdots) \cdot \left(\cos\theta \sin\theta \sin^2\varphi \left(\eta_{\mathrm{ice}} \overline{\overline{\dot{\varepsilon}^{(\mathrm{s})}}}_{12} \right) + \cos\theta \cos\varphi \sin\varphi \left(\eta_{\mathrm{ice}} \overline{\overline{\dot{\varepsilon}^{(\mathrm{s})}}}_{13} \right) \right) \tag{4}$$

Thus, it appears that $\tilde{\sigma}^{\max}(\theta, \varphi)$, as well as $\lambda(\theta, \varphi)$ and $\overline{\overline{M^{(\mathrm{s})}}}$, are explicitly a function of both terms: $\eta_{\mathrm{ice}} \overline{\overline{\dot{\varepsilon}^{(\mathrm{s})}}}_{12}$ and $\eta_{\mathrm{ice}} \overline{\overline{\dot{\varepsilon}^{(\mathrm{s})}}}_{13}$. This allows Eq. (1) to be rewritten as follows:

$$\begin{aligned} \bar{\sigma}_i^{(\mathrm{s})} = 2C_{\mathrm{h}} \Bigg\{ & \overline{\overline{M^{(\mathrm{s})}}}_{i4} \left(\eta_{\mathrm{ice}} \overline{\overline{\dot{\varepsilon}^{(\mathrm{s})}}}_{12}, \eta_{\mathrm{ice}} \overline{\overline{\dot{\varepsilon}^{(\mathrm{s})}}}_{13} \right) \eta_{\mathrm{ice}} \overline{\overline{\dot{\varepsilon}^{(\mathrm{s})}}}_{12} + \cdots \\ & \cdots + \overline{\overline{M^{(\mathrm{s})}}}_{i5} \left(\eta_{\mathrm{ice}} \overline{\overline{\dot{\varepsilon}^{(\mathrm{s})}}}_{12}, \eta_{\mathrm{ice}} \overline{\overline{\dot{\varepsilon}^{(\mathrm{s})}}}_{13} \right) \eta_{\mathrm{ice}} \overline{\overline{\dot{\varepsilon}^{(\mathrm{s})}}}_{13} \Bigg\} \quad (i = 1, \ldots, 6) \end{aligned} \tag{5}$$

But at the steady state, the balance of each snow element I, which is in contact with neither a node nor a pole, is described by the following relationship, which is deduced from Eq. (48) (Part I):

$$\sum_{n=1}^{4} T_I^{n^{(\mathrm{s})}} = -\rho_I V_e g \sin\psi \tag{6}$$

Furthermore, both Eqs. (51) and (52) (Part I) show that both $\overline{\overline{\dot{\varepsilon}^{\mathrm{s}}}}_{12}(H)$ and $\overline{\overline{\dot{\varepsilon}^{\mathrm{s}}}}_{13}(H)$, at a given point H, are linear combinations of the total velocities $\dot{u}_{I_H}$ in direction $\vec{k}_1$, where I_H are snow elements belonging to the vicinity of H. Likewise, both Eqs. (49) and (50) (Part I) express $T_I^{n^{(\mathrm{s})}}$ as a linear combination of $\overline{\overline{\sigma^{(\mathrm{s})}}}_{12}(M_n)$

and $\overline{\overline{\sigma^{(s)}}}_{13}(M_n)$, where points M_n are interpolation points in the vicinity of both nodes I and I_n. Thus, the previous equation (5) makes it possible to establish that $T_I^{n(s)}$ is computed, in a general way, as an explicit one-to-one function f_I^n of the variables $\eta_{ice}\dot{u}_{J_{I,n}}^{(s)}$, where $\dot{u}_{J_{I,n}}^{(s)}$ is the displacement ratio in direction $\vec{k}_1$ of elements $J_{I,n}$ belonging to the vicinity of I and I_n. In these conditions, Eq. (6) may be written in the following form:

$$\sum_{n=1}^{4} f_I^n\left(\eta_{ice}\dot{u}_{J_{I,n}}^{(s)}\right) = -\rho_l V_e g \sin\psi \tag{7}$$

If a snow element I is in contact with a closed section or a pole, the straightforward relation is obtained:

$$\eta_{ice}\dot{u}_I^{(s)} = 0 \tag{8}$$

Eqs. (7) and (8) make up a complete system whose solution $\eta_{ice}\dot{u}_I^{(s)}$ (if this solution exists) does not depend on K_{ice}, nor on η_{ice}. Likewise, from Eq. (5), as $\bar{\sigma}_i^{(s)}$ is only a function of $\eta_{ice}\overline{\overline{\dot{\varepsilon}^{(s)}}}_{12}$ and $\eta_{ice}\overline{\overline{\dot{\varepsilon}^{(s)}}}_{13}$, it can be deduced that $\bar{\sigma}_i^{(s)}$ as well as any term $T_I^{n(s)}$ depend neither on K_{ice}, nor η_{ice}. Thus, forces applied to the nodes of the net or to the poles depend on neither K_{ice}, nor η_{ice}.

This is a fundamental result, since it means that the forces existing in the different parts of the structure do not depend on the constitutive parameters of the snowpack, but only on the physical parameters such as the coordinate number or the number of grain bonds per unit of volume, as well as on the density profile of the snowpack. As will be established in a further section, this feature substantially reduces the computation time. For engineering purposes, this is of course of great practical interest. Nevertheless, it must be noted that this result is not general but must be regarded as a mathematical consequence of the form of the constitutive relations. We emphasize that this important result is rigorously unchanged if the exponent α_{ice} is chosen different from 1. In the general non-linear case, forces acting within the structure will be a function only of exponent α_{ice}, but not of K_{ice}, nor of η_{ice}.

As outlined in Part I, a complex overall behaviour is obtained for the snowpack by taking a statistical description of the fabrics into account. This statistical description lies essentially in both distribution functions, namely f_θ and f_φ. Since failure may occur between two contact grains, functions f_θ and f_φ may change. Hereafter, in order to exemplify using simplistic but meaningful modelling, these functions will be considered to remain uniform. This is made possible by imposing a sufficiently large failure stress $\tilde{\sigma}_l$. This oversimplification prevents the micro-structure of the medium from changing during the transient phase. This is certainly not exact, but must be regarded as a first and useful approximation to investigate the capability of the complete model. Interestingly, analytical investigations were performed on the influence of the failure on grain bonds (Nicot, 2003).

3. A double time-step numerical scheme

3.1. Introduction

A general balance equation such as Eqs. (48) and (53) (Part I) can be written with the following general formulation:

$$\ddot{q}_l = f(q_m, \dot{q}_m) \tag{9}$$

Each variable q_l, which represents one of the location coordinates of a node of the net sheet or the displacement of a snow element, is a function of a set of other variables generally denoted q_m. These variables may be the location coordinates of a node of the net sheet, the displacement of a snow element, as well as the reaction force existing between a node of the net sheet and a snow element that are in contact. An

explicit numerical algorithm was developed that introduces time sampling of general equations using the explicit finite differences method. Thus, a set of explicit equations was obtained:

$$\dot{q}_l(t+\tau) = \dot{q}_l(t) + \tau f\left(q_m(t), \frac{q_m(t) - q_m(t-\tau)}{\tau}\right) \tag{10}$$

$$q_l(t+\tau) = q_l(t) + \tau \dot{q}_l(t+\tau) \tag{11}$$

where τ is the time step. At each time loop, the algorithm allows the displacements of every body to be computed as a function of their previous positions. This numerical process continues until an equilibrium state between the mantel and the structure is obtained.

3.2. Time sampling

The displacement of the snow element I in contact with a node J, is described by Eq. (48) (Part I). If this element is not in contact with a node, Eq. (48) remains valid by setting $R_I(t) = 0$; if this element is in contact with a pole, thus $u_I(t) = 0$ and $R_I(t) = \rho_l V_e g \sin\psi + \sum_{n=1}^{4} T_I^n(t)$. In the most general case, the snow element I is in contact with a closed section J. Time sampling on Eq. (48) (Part I), with time step τ_s, provides the following equation at time t:

$$\dot{u}_I(t+\tau_s) = \dot{u}_I(t) + g\sin\psi\tau_s + \frac{\tau_s}{\rho_l V_e}\left(\sum_{n=1}^{4} T_I^n(t) - R_I(t)\right) \tag{12}$$

$$u_I(t+\tau_s) = u_I(t) + \tau_s \dot{u}_I(t+\tau_s) \tag{13}$$

Likewise, time sampling on Eq. (53) (Part I), with time step τ_n, provides the following equations at time t:

$$\dot{\vec{X}}_J(t+\tau_n) = \dot{\vec{X}}_J(t) + g\sin\psi\tau_n + \frac{\tau_n}{m}\left(\sum_{j=1}^{6} \vec{F}_J^j(t) + R_I(t)\vec{k}_1\right) \tag{14}$$

$$\vec{X}_J(t+\tau_n) = \vec{X}_J(t) + \tau_n \dot{\vec{X}}_J(t+\tau_n) \tag{15}$$

The numerical stability of all equations (12)–(15) requires choosing time steps τ_s and τ_n that are small enough. Denoting τ_s^* and τ_n^* the values of τ_s and τ_n, which ensure numerical stability, the usual values for Youngs modulus E of steel and Youngs modulus K_{ice} induce an important shift between τ_s^* and τ_n^*: τ_n^* is very small compared to τ_s^*. Making use of the fact that at the steady state the forces acting within the structure are not a function of K_{ice}, nor of η_{ice}, this shift is all the greater since a very small K_{ice} can be chosen.

Imposing $\tau_n = \tau_s = \tau_n^*$, allows us to consider the interaction between the snowpack and the structure at a given time t. It must be noted that this choice is likely to induce a time-consuming computation. During the period between t and $t + \tau_s^*$, the snowpack is strained, and thus it directs a displacement of the nodes of the structure. As dynamic effects can be neglected, the mechanical response of the structure would not have been modified if the strain within the snowpack had occurred over a shorter period τ_n^* between t and $t + \tau_n^*$. This condition can be written from Eq. (55) (Part I) as follows:

$$\tau_s^* \dot{u}_I(t) = \tau_n^* \dot{\vec{X}}_J(t) \cdot \vec{k}_1 \tag{16}$$

In these conditions, both positions and velocities of each node at time $t + \tau_s^*$ would have been unchanged if the following process had taken place between t and $t + \tau_s^*$:

- $\vec{X}_J(t+\tau_n^*)$ and $\dot{\vec{X}}_J(t+\tau_n^*)$ are computed by Eqs. (14) and (15), taking Eq. (16) into account.
- The following equalities are imposed:

$$\dot{\vec{X}}_J\left(t+\tau_s^*\right)=\dot{\vec{X}}_J\left(t+\tau_n^*\right) \tag{17}$$

$$\vec{X}_J\left(t+\tau_s^*\right)=\vec{X}_J\left(t+\tau_n^*\right) \tag{18}$$

Thus, the set of Eqs. (12)–(15) can be rewritten as follows:

$$\dot{u}_I\left(t+\tau_s^*\right)=\dot{u}_I(t)+g\sin\psi\tau_s^*+\frac{\tau_s^*}{\rho_I V_e}\left(\sum_{n=1}^{4}T_I^n(t)-R_I(t)\right) \tag{19}$$

$$u_I\left(t+\tau_s^*\right)=u_I(t)+\tau_s^*\dot{u}_I\left(t+\tau_s^*\right) \tag{20}$$

$$\dot{\vec{X}}_J\left(t+\tau_s^*\right)=\dot{\vec{X}}_J(t)+g\sin\psi\tau_n^*+\frac{\tau_n^*}{m}\left(\sum_{p=1}^{6}\vec{F}_J^p(t)+R_I(t)\vec{k}_1\right) \tag{21}$$

$$\vec{X}_J\left(t+\tau_s^*\right)=\vec{X}_J(t)+\tau_n^*\dot{\vec{X}}_J\left(t+\tau_s^*\right) \tag{22}$$

The set of Eqs. (19)–(22) constitutes a numerical scheme, which introduces two time steps: τ_s^* and τ_n^*. However, the period for calculating new positions of each body is equal to τ_s^*, optimising the computation time. Typically, for the simulations described in the last section, the computation time can be reduced by approximately a factor of 100, from 4 days to less than a hour.

3.3. A complete equation system

The kinematic condition given by Eq. (16) allows the reaction force $R_I(t)$ to be derived:

$$\begin{aligned}R_I(t)=\frac{1}{\frac{\tau_s^{*2}}{\rho_I V_e}+\frac{\tau_n^{*2}}{m}}\Bigg\{&\tau_s^*\dot{u}_I(t)+\tau_n^*\dot{\vec{X}}_J(t)\cdot\vec{k}_1+\frac{\tau_s^{*2}}{\rho_I V_e}\sum_{n=1}^{4}T_I^n(t)+\cdots\\&\cdots+g\sin\psi\left(\tau_s^{*2}-\tau_n^{*2}\right)-\frac{\tau_n^{*2}}{m}\sum_{p=1}^{6}\vec{F}_J^p(t)\cdot\vec{k}_1\Bigg\}\end{aligned} \tag{23}$$

The set of Eqs. (19)–(23) provides the position of each snow element I, as well as the position of each node J, to be computed explicitly at any time. If a node I (resp. element J) is not in contact with an element J (resp. node I), both Eqs. (19) and (20) (resp. (21) and (22)) remain relevant by setting $R_I(t)$ equal to zero. Once an equilibrium state between the structure and the snowpack is obtained, terms $R_I(t)$, $T_I^n(t)$ and $\vec{X}_J(t)$ remain constant, and thus the final forces acting in different parts of the structure can be computed.

4. Optimal size of snow elements

4.1. Influence of the size of snow elements

The numerical algorithm has led to the development of computational software so that avalanche nets can be easily designed as a function of the upstream snow conditions. It is possible to simulate several successive snow scenarios: by changing the number of layers, their height, their density or their physical

parameters, snowfalls or melting with settlement can be simulated. Thus, this tool allows engineers to predict the mechanical behaviour of the structure during usual or unusual climatic situations.

Hereafter, the influence of the magnitude of the snow elements on the numerical solution will be analysed. A very simple structure is used, composed of a square panel of net, whose lateral sides are fixed to a post, with the two others free. In order to simplify the problem, it is assumed that the snowpack is vertically disposed above the net, which is in a horizontal configuration (Fig. 1). The snowpack is retained not only by the net sheet (at the nodes of the mesh), but also by the posts (because of the gliding between the snow elements and the posts). The four vertical sides of the snowpack are assumed to be free. The snowpack, whose density is equal to 500 kg/m^3, is 0.7 m high by 0.7 m wide and 20 m long. The net mesh comprises 49 nodes. Several simulations were performed by changing the magnitude of the snow elements. For these simulations, it was assumed that the width and the height were equal:

$$w_e = h_e = \omega \tag{24}$$

and a set of rising values of ω was computed. It is meaningful to define the dimensionless ratio $\varpi = l_0/\omega$, where $l_0 = 0.1$ m is the usual size of the net mesh. Typically, values of ϖ belonging to the range [5–200] were used. Above $\varpi = 200$ ($\omega = 0.005$ m), the computation is excessively time-consuming; below $\varpi = 5$ ($\omega = 0.02$ m), the size of elements is likely to be too large with regard to the size of the net mesh. Furthermore, as mentioned in Part I, $\omega = 0.02$ m can be regarded as the smallest size of snow elements, which ensures that the RVE is entirely contained into the volume of a snow element.

As presented in Part I, the interaction between the snowpack and the net sheet is obviously not reduced to a single point. The wires that comprise the net sheet have a cross-section that should not be ignored. Thus, a closed section S_c is associated with each node of the net mesh. An initial section is considered, taking only the mean cross-section of the wires into account; this section is denoted S_0. As a first step, it is assumed that S_0 and S_c are equal. The following paragraph will be devoted to the influence of the value of S_c. Likewise, the exponent α_{ice} was chosen equal to 1. A further parametric analysis will make it possible to assess the influence of the exponent α_{ice}.

To compare the results of the several simulations, we considered the resultant force F_{pole} applied to the two horizontal poles and the resultant force F_{net} accounting for all the reaction forces acting on the different nodes of the net. Fig. 2 shows the changes in F_{net} and F_{pole} as a function of ϖ. It can be observed that both

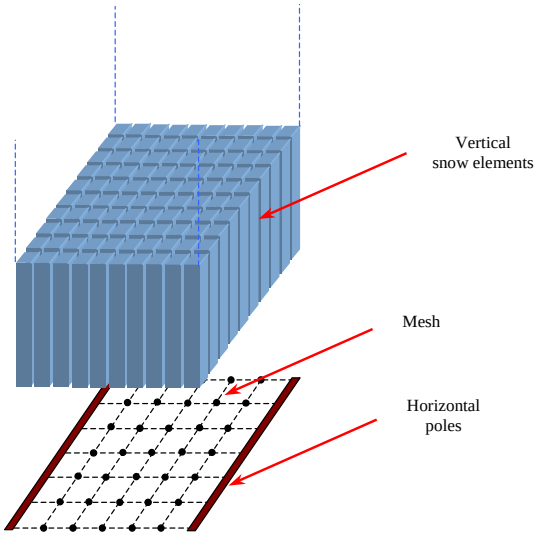

Fig. 1. Geometrical configuration of the simplistic model.

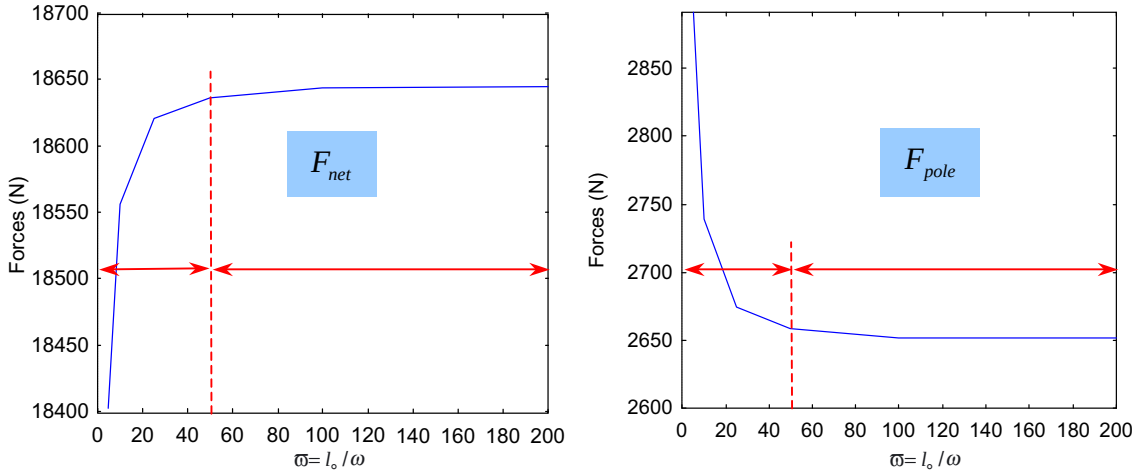

Fig. 2. Changes in the forces acting on the structure as a function of ϖ.

F_{net} and F_{pole} change substantially while ϖ is lower than 50 (which corresponds, as $l_0 = 0.1$, to $\omega > 0.002$ m). When ϖ is greater than 50, the forces acting on the anchors or on the poles remain approximately constant. Thus, the asymptotic value can be regarded as the solution to the problem. Nevertheless, it must be noted that the changes in F_{net} and F_{pole} remain lower than 10% when ϖ increases from 5 to 200. Values obtained when $\varpi = 5$ provide a rather good approximation of the solution. Furthermore, this value of ϖ seems to be a good compromise for optimising computation time. In what follows, further simulations will be performed setting $\varpi = 5$, which corresponds to $\omega = 0.02$ m.

4.2. Influence of the permeability of the net sheet

The influence of the closed section will now be analysed. A current section S_c is considered with $S_c = a_S S_0$ where the parameter a_S belongs to the range [0.1–2]. The interaction between the snow elements and the wires is modelled by considering that elements which are located upstream of a closed section, associated with each node of the wire mesh, are blocked; the closed section accounts for the longitudinal section of the adjoining wires. Of course, as mentioned in Part I, this is a simplistic description of what actually occurs. Thus, it seems meaningful to consider that the parameter a_S can be different from the value 1: the range [0.1–2] is therefore investigated. For instance, in the previous section, a_S was chosen equal to 1. The previous simplistic model, described in Fig. 1, is considered again, with $\omega = 0.001$ m ($\varpi = 100$). The changes in the resultant force F_{pole} applied to the two poles as a function of parameter a_S are analysed. As depicted in Fig. 3, a strong influence of parameter a_S is observed. This influence is more important when parameter a_S is small (lower than 0.5). For the parameter a_S belonging to the range [0.5–2], a relative variation of 25% around the value obtained with $a_S = 1$ is observed. This feature has two consequences:

- It seems to be realistic to limit the range of parameter a_S to [0.5–2], but it must be noted that this choice can be risky. In these conditions, it seems relevant to use the central value $a_S = 1$, which corresponds to the mean value of F_{pole}. Consequently, an uncertainty of around 25% must be associated with the final result.
- As shown in Fig. 2, the error induced by the size of the snow elements does not exceed 10% if ϖ is not lower than 5. This error is lower than the uncertainty due to parameter a_S. A greater value of ϖ would improve the precision of the result, but the substantial gain in precision, which requires time-consuming

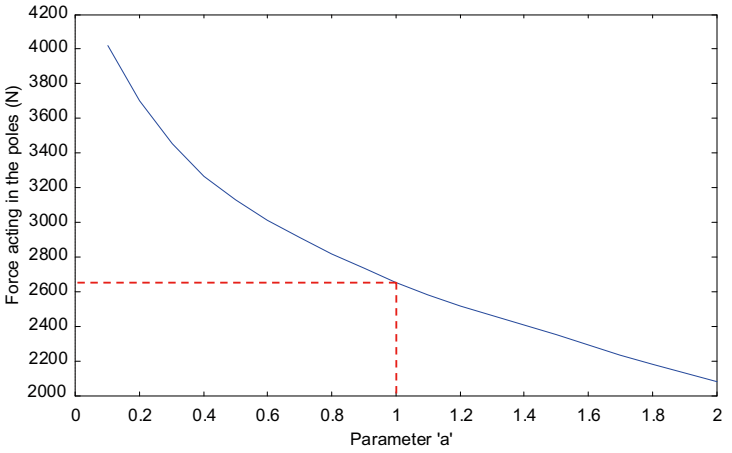

Fig. 3. Influence of the size of the closed section at the interface.

computations, would be counterbalanced by a excessively great uncertainty (25%) due to a_S, which is difficult to reduce. Because forces acting in the structure dramatically increase when ϖ is lower than 5, a value of ϖ lower than 5 would be likely to induce an error greater than the initial 25%. Thus, it can be concluded that the choice of $\varpi = 5$ appears to be a good compromise for defining the size of the snow elements.

In later sections, values $\varpi = 5$ and $a_S = 1$ will be adopted.

4.3. Influence of the exponent α_{ice}

Further simulations were carried out with the exponent α_{ice} varying in the range of [0.1–5]. As discussed in Part I, the lack of knowledge on the bond-scale structure of the ice makes it difficult to calibrate the

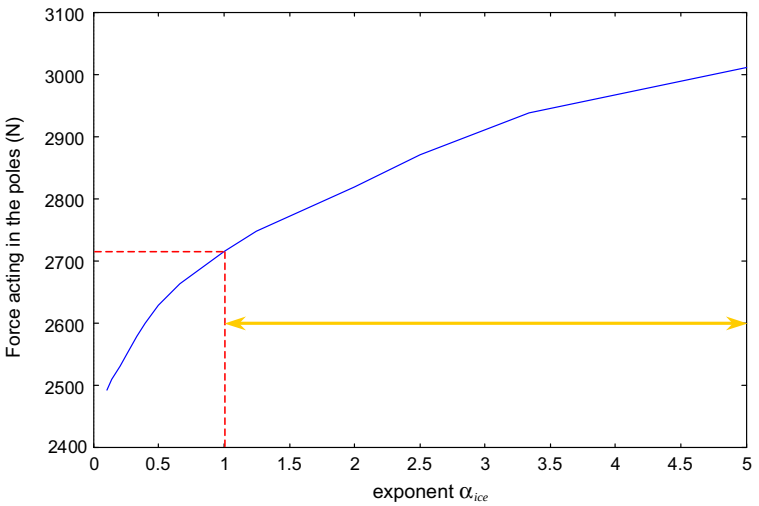

Fig. 4. Influence of the exponent α_{ice}.

exponent α_{ice}. Nevertheless, it seems reasonable to consider that α_{ice} can vary in the range of [1–5] (Gagliardini and Meyssonnier, 1999). In particular, in Glen's law for creep, $\alpha_{ice} \approx 3$. Fig. 4 shows that the smaller this exponent is, the greater the influence of α_{ice} is, typically $\alpha_{ice} < 1$. Furthermore, denoting $\overline{F}_{pole}$ the value of F_{pole} when $\alpha_{ice} = 1$, it must be noted that the relative variation of F_{pole}, which can defined as $|F_{pole} - \overline{F}_{pole}|/\overline{F}_{pole}$, does not exceed 10% when α_{ice} varies in the usual range of [1–5]. This is an interesting result; indeed, in as much as it can be assumed that no failure can occur inside grain bonds, this result establishes that the influence of the exponent α_{ice} remains very small, and lower than the uncertainty caused by other parameters such as a_S . This justifies using a linear local constitutive law to model the mechanical interaction between a snowpack and a flexible structure. In this kind of problem, considering the assumptions used to describe the macroscopic strain field of the snowpack, more complex local constitutive models are not likely to bring a significant improvement in the final result. Thus, for the further simulations, values $\varpi = 5$, $a_S = 1$ and $\alpha_{ice} = 1$ will be adopted.

5. First elements of validation

During the winter of 1999–2000, several snow avalanche net structures were monitored in the French Alps. Force sensors were mounted in order to record the changes in the forces acting on the upstream anchors. The analysis of the experimental results showed that those at the Flaine (Haute–Savoie) site provided the most reliable and useable results; the data from this site were consequently chosen for analysis. In what follows, the situation observed on 12 April 2000 is considered. The height of the snow mantel was equal to 3.58 m, and the average density was equal to 560 kg/m^3. These values were measured 4 m upstream from the poles. Fig. 5 shows the geometrical description of the structure.

To perform the numerical simulation, a single-layer snowpack was studied, with $N_b^0 = 1000$ and $\bar{n}_c = 5$. The snow elements were 0.02 m high by 0.02 m wide by 11 m long. The friction angle φ_s between the soil and the snowpack was chosen equal to 20°. A comparison between experimental and numerical values of the forces acting on the upstream anchors is presented in Table 1. A rather good agreement between experimental and numerical values can be seen for the both internal and pre-external anchors (see Fig. 7, Part I). However, a large divergence must be noted for the external anchors. Nevertheless, the small experimental value recorded in the external anchor looks suspicious. Generally, the maximal force is located in the

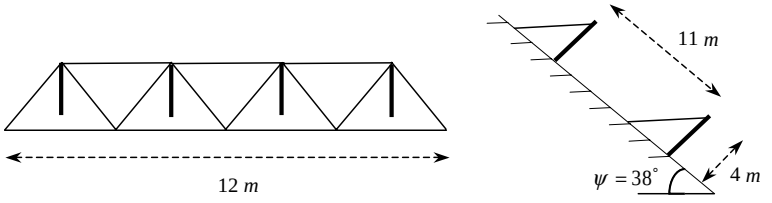

Fig. 5. Geometrical configuration of the structure.

Table 1
Comparison of experimental and numerical results

	Internal anchor	Pre-external anchor	External anchor
Experimental result (kN)	95	111	67
Numerical result (kN) (free lateral planes)	110	109	153
Numerical result (kN) (blocked left lateral plane)	106	102	123

external anchor (Margreth, 1995). This divergence is partly caused by the strong irregularities in topography near the external anchor: the presence of a rocky crest is likely to influence the stabilization of the snowpack. Indeed, the results are slightly better while the lateral plane is blocked. The next monitoring of a structure at the Tignes site (Savoie, France), which is set up in a very smooth and regular area, should provide further valuable experimental data beginning in 2004. At present, the good agreement for both the internal and the pre-external anchors should be considered as a first element of validation.

The distribution of the pressure applied to an external pole is shown in Fig. 6. It can be noted that the shape of this distribution is approximately linear from the ground surface up to 2 m in height. Above this height, the pressure increases strongly. Interestingly, the uniform pattern of pressure applied to the poles, required by the Swiss Guidelines (Margreth, 1990) for designing protective barriers, is not confirmed by the proposed numerical simulations. Unfortunately, the poles were not monitored, so that this numerical result cannot be compared to the experimental data. As the distribution of the pressure has a substantial influence on the poles' bending moment, it strongly governs the design of these poles. Further experimental investigations will therefore be carried out to make such data available in the future. Fig. 7 shows the dis-

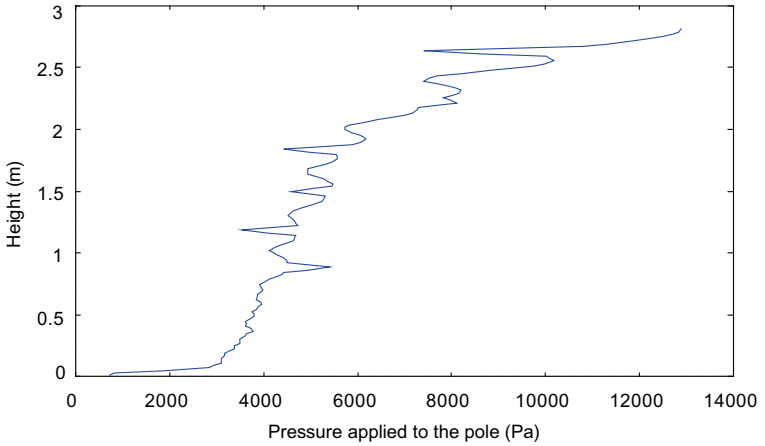

Fig. 6. Distribution of the pressure applied to the poles.

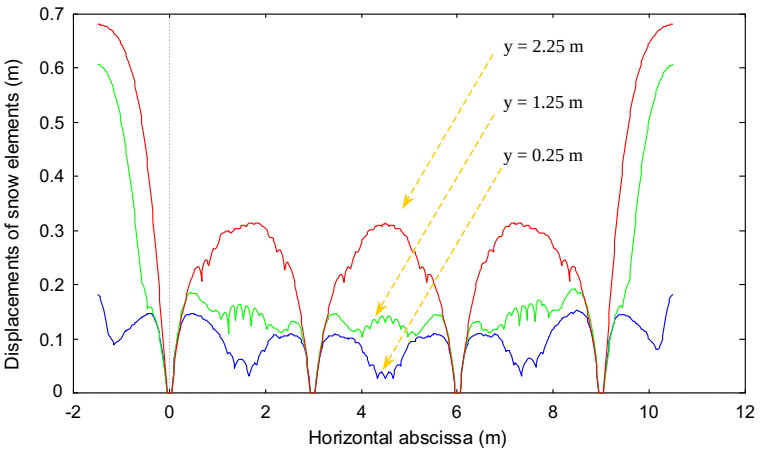

Fig. 7. Displacement field into the snowpack.

placement field of the snowpack in several planes parallel to the ground surface: at a 0.25 m depth, a 1.25 m depth and a 2.25 m depth. The displacements decreased with the depth and were equal to zero behind the poles. Of course, it must be noted that this displacement field results from the assumptions concerning the kinematics of the snow elements: in particular, they are perfectly rigid in compression, so that the displacement field does not depend on x_1.

6. An example of an advanced simulation

In order to show the capabilities of the computational software, a complete simulation will be described in this section. Typical successive meteorological events are explained. The structure is composed of a line of four poles. The height of the net sheet is equal to 4 m. Each pole, which is hollow, has a diameter of 168.3 mm and a wall thickness of 4.5 mm. The distance between two adjoining poles is 3.50 m. The slope above the structure is 45°. The geometrical settings of the structure are described in Fig. 8.

As depicted in Fig. 9, two successive snow situations were analysed. First, a three-layer mantel was considered, in which a recent snow layer and an old dense snow layer are separated by a thin layer. This situation is typical of February in the French Alps. Second, a two-layer mantel was examined, whose snow layers were very dense. This is the usual spring situation: the snowpack has been subjected to the effect of melting and settlement. Even if the height of the mantel is lower in the second case, the total weight of the mantel remains unchanged. Although this feature may not occur, it was adopted in order to examine the sole influence of the height of the mantel.

To perform the two numerical simulations, the number of grain bonds in a RVE was fixed at 1000. The snow elements measured 0.02 m high by 0.02 m wide by 25 m long. The friction angle φ_s between the soil and the snowpack was chosen equal to 20°. During densification, the coordination number rises; thus, this parameter should vary with layers. Nevertheless, for the sake of simplicity, a simplistic choice of $\bar{n}_c$ was

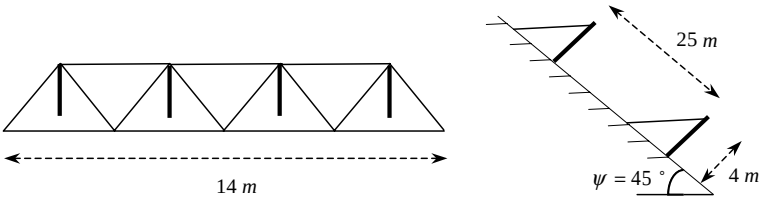

Fig. 8. Geometrical configuration of the structure.

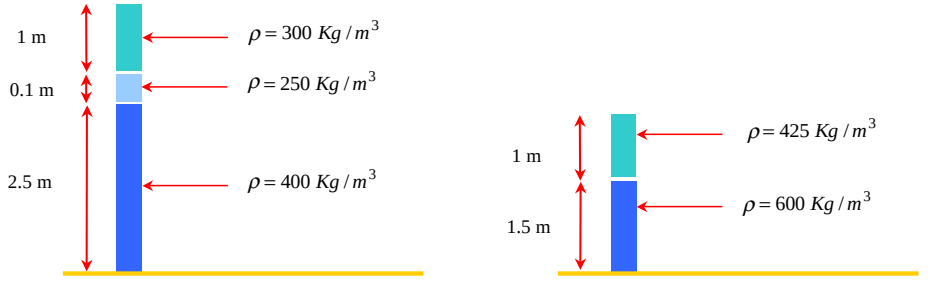

Fig. 9. Changes in a layered mantel between February and April.

Table 2
Forces acting in the anchors: comparison between February and April situations

	Forces (kN)		
	Internal anchor	Pre-external anchor	External anchor
February situation	261	260	298
April situation	242	240	285

made: in the two upper layers of the first mantel (February), $\bar{n}_c = 3$; in the other layers, in February or April, as the density is greater than 400 kg/m^3, $\bar{n}_c = 5$ (Brown and Edens, 1991).

Table 2 compares the forces acting in the anchors in the course of the two situations. It can be observed that the forces are slightly greater in the first situation. Even if the weight of the mantel is identical for the two scenarios, the first loading induces the strongest forces. That means that the forces acting on the anchors are a function of the weight of the mantel, $W = \sum_{l=1}^{n_l} \rho_l w h_l L$, but also of the total height of the mantel, $H = \sum_{l=1}^{n_l} h_l$. This can be expressed as follows:

$$F_a(i) = f_i(W, H) \tag{25}$$

where $F_a(i)$ is the resulting force acting in the anchor 'i', and f_i is a non-linear operator that depends on the position of the anchor (external, pre-external or internal anchor). Implicitly, this operator takes the final strained geometrical configuration of the structure into account. The non-linearity of f_i is mainly caused by the geometrical non-linearities occurring in the course of the deformation of the structure.

Recent research (Gay and Nicot, 2001) has shown that the operator f_i can be assessed using the following straightforward power law expression:

$$F_a(i) = aW^b H^c \tag{26}$$

with $b \approx 1$ and $0 < c < 1$.

For the case considered, $F_a(1) = 1.64W\ H^{0.21}$ for both the internal and the pre-external anchors, and $F_a(2) = 2.02W\ H^{0.12}$ for the external anchors.

The comparison of the pressure applied to the poles is illustrated in Fig. 10. First, the curve corresponding to the February situation shows that the presence of a thin light layer induces a strong decrease in the pressure. Thus, because of the influence of the layering of the mantel, it is of great importance to have a

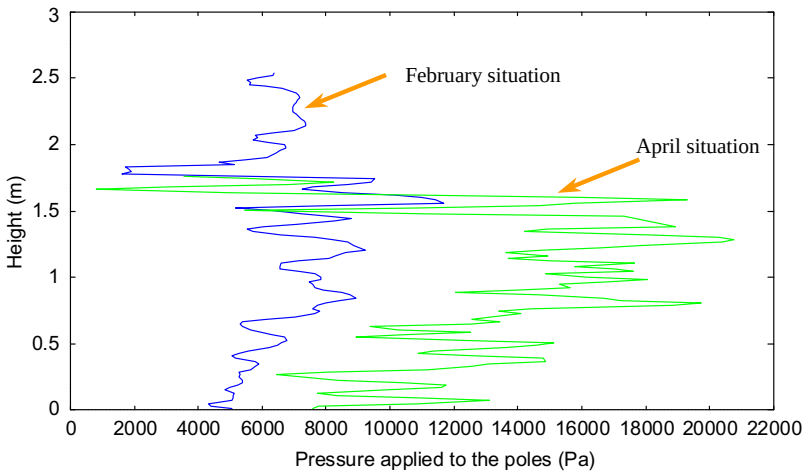

Fig. 10. Distribution of the pressure applied to the poles.

physical description that is as accurate as possible. Furthermore, it can be observed that the pressure corresponding to the April situation is the greater of the two. Thus, the loading applied by a snowpack to the poles seems to depend substantially on the height of the mantel. During the settlement of the snow cover, if the total weight of the mantel remains unchanged, the pressure applied to the poles is likely to increase dramatically. This makes it even more important to perform several simulations with different successive realistic snow conditions in order to determine the most severe situation. Taking this situation into account will provide an effective design of the protective structure. As depicted in Fig. 10, strong oscillations occur in the pressure profile. These oscillations seem to be related to the discrete representation of both the wire net and the snowpack. As the interaction between both the wire mesh and the snow elements is modelled using a powerful kinematic condition, the velocity field within the snowpack is substantially discontinuous. As the pressure applied to the poles is computed from the velocity of the snow elements which are in contact with those located upstream from the poles, the discontinuous nature of the velocity field then directs oscillations in the pressure profile. Actually, the velocity field within the snowpack is likely to be smoother, and discontinuities do not occur, except perhaps in the vicinity of the physical discontinuities of the snowpack (interfaces between adjoining layers). So large oscillations therefore result from the nature of the modelling system, but are not likely to correspond to a physical phenomenon. Nevertheless, the simulated pressure profile brings some valuable mean information, which can be sufficient to design the structure: further mathematical treatment (a filtering process) can be used in order to regularize the profile.

7. Concluding remarks

The actual complexity that engineers face in assessing the loading applied by a snow mantel requires a specific research program that will attempt to develop a coupled mechanical analysis of both the structure and the snow mantel by scientifically analyzing the interaction between the snow mantel and the structure. This paper has proposed an original approach based on the discrete element method (Cundall and Roger, 1992) to model both the structure and the snowpack. Because of the particular form of the displacement field within the snowpack, it has been shown that this type of model was well adapted. As the equilibrium state between the snowpack and the structure does not depend on the mechanical parameters used in the constitutive model, a useful double time-step numerical scheme was developed, allowing computation time to be greatly optimized.

This complete modelling was integrated into computational software, allowing avalanche net structures to be designed according to snow conditions. Thus, various snow conditions, which can be related to meteorological scenarios, can be simulated.

Finally, the forces acting on a protective structure can be understood as the final result of a chain gathering complex phenomena: (i) snowfalls; (ii) physical changes in the snowpack in interaction with the climatic conditions, the ground surface, and a flexible structure; (iii) the mechanical behaviour of a flexible structure. As a direct experimental study of the snowpack remains a very difficult task, a structure for indirectly obtaining information related to the snowpack appears to be extremely useful. In these conditions, the net structure functions as a macroscopic but relevant sensor. This paper presents the first step of this original approach.

References

Brown, R.L., Edens, M.Q., 1991. On the relationship between neck length and bond radius during compression of snow. Journal of Glaciology 37 (126), 203–208.

Cundall, P.A., Roger, D.H., 1992. Numerical modelling of discontinua. Engineering Computations 9, 101–113.
Gagliardini, O., Meyssonnier, J., 1999. Analytical derivations for the behavior and fabric evolution of a linear orthotropic ice polycrystal. Journal of Geophysical Research 104, 17,797–17,809.
Gay, M., Nicot, F., 2001. Interaction between a snowpack and defensive net fences. In: Seminar on Snow and Avalanches Test Sites, Grenoble, October 2001. Cemagref Ed.
Margreth, S., 1990. Directives pour la construction d'ouvrages paravalanches dans la zone de décrochement. Institut fédéral pour l'étude de la neige et des avalanches, Ed. OFEFP.
Margreth, S., 1995. Snow Pressure Measurements on Snow Net Systems. Actes de colloque, Chamonix. pp. 241–248.
Nicot, F., 2003. Constitutive modelling of a snowcover with a change in scale. European Journal of Mechanics (A/Solids) 22 (3), 325–340.